HHS Public Access

Author manuscript

Ultrasound Med Biol. Author manuscript; available in PMC 2020 September 01.

Published in final edited form as:

Ultrasound Med Biol. 2019 September ; 45(9): 2515–2524. doi:10.1016/j.ultrasmedbio.2019.04.027.

Assessment of the Superharmonic Response of Microbubble Contrast Agents for Acoustic Angiography As A Function of Microbubble Parameters

Isabel G. Newsome[a], **Thomas M. Kierski**[a], **Paul A. Dayton**[a,*]

[a]University of North Carolina and North Carolina State University, Joint Department of Biomedical Engineering, CB 7575, Chapel Hill, NC 27599, USA

Abstract

Acoustic angiography is a superharmonic contrast-enhanced ultrasound imaging technique that enables 3D, high-resolution microvascular visualization. This technique utilizes a dual-frequency imaging strategy, transmitting at a low frequency and receiving at a higher frequency to detect high frequency contrast agent signatures and separate them from tissue background. Prior studies have illustrated differences in microbubble scatter dependent on microbubble size and composition; however, most previously reported data has utilized a relatively narrow frequency bandwidth centered around the excitation frequency. To date, a comprehensive study of isolated microbubble superharmonic responses with a broadband dual-frequency system has not been performed. Here, the superharmonic signal production of 14 contrast agents with various gas cores, shell compositions, and bubble diameters at mechanical indices of 0.2 to 1.2, was evaluated using a transmit 4 MHz, receive 25 MHz configuration. Results indicate that perfluorocarbon cores or lipid shells with 18- or 20-carbon acyl chains produce more superharmonic signal than sulfur hexafluoride cores or lipid shells with 16-carbon acyl chains, respectively. As microbubble diameter increases from 1 to 4 μm, superharmonic generation decreases. In a comparison of two clinical agents, Definity and Optison, and a preclinical agent, Micromarker, Optison produced the smallest superharmonic signals. Overall, this work suggests that microbubbles around 1 μm in diameter with perfluorocarbon cores and longer-chained lipid shells perform best for superharmonic imaging at 4 MHz. Studies demonstrate that microbubble superharmonic response follows different trends than shown in prior studies using a narrower frequency bandwidth centered around the excitation frequency. Future work will apply these results *in vivo* to optimize the sensitivity of acoustic angiography.

Keywords

microbubble; ultrasound; acoustic angiography; superharmonic; perfluorocarbon

*Corresponding author: padayton@email.unc.edu, 919-843-9521.

Introduction

Since the first use of microbubbles for ultrasound contrast enhancement (Gramiak and Shah 1968), microbubble contrast agents have become a common tool in clinical use and preclinical research worldwide. Several contrast agents are now commercially available and routinely used in the clinic. A recent evaluation of the most common clinical agents in the United States found differences in performance of these agents at the clinical dose (Hyvelin et al. 2017). As the field of contrast-enhanced ultrasound has grown, studies have been published on methods of microbubble synthesis (Feshitan et al. 2009; Lee et al. 2017) and contrast-specific techniques, such as harmonic imaging (Frinking et al. 2000), subharmonic imaging (Shi et al. 1999; Sridharan et al. 2013), pulse-inversion imaging (Eckersley et al. 2005; Shen et al. 2005), and combinations of these methods. Applications of these contrast-specific techniques include perfusion imaging (Feingold et al. 2010; Fröhlich et al. 2015; Hudson et al. 2009) and molecular imaging (Abou-Elkacem et al. 2015; Kaufmann et al. 2007; Streeter et al. 2010; Tsuruta et al. 2017).

Superharmonic imaging is an extension of harmonic imaging that has been developed to take advantage of the broadband frequency response of microbubbles, with the goal of achieving signal separation between the excitation signal and scattered bubble responses (Bouakaz et al. 2002; Gessner et al. 2013; Kruse and Ferrara 2005). One such method optimally uses dual-frequency transducers to excite microbubble contrast at a low frequency (4 MHz) and receive the superharmonic response at a much higher frequency (25–30 MHz) (Gessner et al. 2013). By doing so, the acoustic signals of microbubbles are isolated from the signals of tissue, creating detailed, high-resolution maps of the microvasculature (Gessner et al. 2013). Applications of this approach in 3D enable “acoustic angiography,” which provides volumetric imaging of microvascular patterns akin to computed tomography angiography, yet with contrast ultrasound (Gessner et al. 2012). Previous work has focused on optimizing microbubble response for this technique, examining contrast-to-tissue ratio as a function of peak negative pressure for varying transmit frequencies, contrast concentrations, and microbubble diameters (Lindsey et al. 2014). A similar study investigated the generation of superharmonic energy from microbubbles, finding that shell fragmentation creates the strongest superharmonic signals (Lindsey et al. 2015a). To date, clinical implementation of acoustic angiography has demonstrated that increased signal-to-noise ratio would improve the utility this technique in human use where contrast dose is regulated (Shelton et al. 2017). One means to achieve a superharmonic signal increase might be to use optimally-sized microbubble contrast agents, as it is well known that the microbubble diameter can influence scattered signal intensity (Kaya et al. 2010; Segers et al. 2018; Sirsi et al. 2010; Streeter et al. 2010; Talu et al. 2008). We also note that composition of the encapsulating shell and gas core of microbubbles may affect echogenicity. Previous studies have suggested increased microbubble stability (Garg et al. 2013) and nonlinear response (Van Rooij et al. 2015) with increasing acyl chain length of the main phospholipid in the encapsulating shell. However, to date, a comprehensive study of the superharmonic signal produced as a function of microbubble and acoustic parameters has not been performed. Thus, the purpose of the present work is to evaluate differences in superharmonic signal production across various types and sizes of contrast agents under conditions of varying acoustic pressure and to

establish which agent might provide the best performance for acoustic angiography and similar applications.

Materials and Methods

Contrast Agent Preparation

The microbubble contrast agents tested in this work are summarized in Table I. In-house microbubble contrast was formulated as described previously (Shelton et al. 2015). Briefly, dried lipids were dissolved in a mixture of phosphate buffered saline (PBS), propylene glycol, and glycerol at the molar ratios and volume percentages described in Table II. The lipid solution was then aliquoted into vials, the headspace in each vial was exchanged with a selected gas as listed in Table I, and each vial was shaken with a mechanical agitator (Vialmix, Lantheus Medical Imaging, North Billerica, MA, USA) to form polydisperse, lipid-shelled microbubbles. Several commercially-available contrast agents were used in addition to those formulated in-house: Optison (GE Healthcare, Inc., Marlborough, MA, USA), Definity (Lantheus Medical Imaging, Inc., North Billerica, MA, USA), Micromarker (FUJIFILM VisualSonics, Inc., Toronto, ON, Canada), and a variety of preclinical size-isolated microbubbles (SIMBs, Advanced Microbubbles Laboratories, Boulder, CO, USA). Clinical agents were prepared according to manufacturer-provided instructions (Optison package insert 2016; Definity package insert 2017).

In total, the fourteen contrast agents used were separated into four groups for comparison: 1) clinical and preclinical, 2) bubble diameter, 3) gas core, and 4) lipid shell. Table I lists the contrast agents chosen for each group. Although SIMBs are a preclinical agent, in this work, they were used specifically for examining the effect of microbubble diameter and were not compared in the clinical and preclinical group. To examine the effect of lipid composition, four lipid formulations were tested with varying acyl chain lengths: 1) C16–2L and 2) C16–3L, both with 16 carbons in their acyl chains; 3) C18–2L, which has an 18-carbon acyl chain; and 4) C20–2L, aptly named for its 20-carbon acyl chain. More detail on these formulations can be found in Table II. Microbubbles with the same shell (the in-house lipid formulation referred to as C18–2L) and either octafluoropropane (C_3F_8 or “OFP”), decafluorobutane (C_4F_{10} or “DFB”), or sulfur hexafluoride (SF_6) as the gas core were compared to evaluate the effect of gas core composition. The concentration and size distribution of all contrast agents were measured with a single particle optical sizing device (0.5 to 400 μm measurable range, Accusizer 780A, Particle Sizing Systems, Santa Barbara, CA, USA). In this work, we have focused on quantifying superharmonic production from a population of bubbles, where the size of the population (i.e. #/mL) is a constant variable across all measurements. As such, all concentration and size measurements presented are number- rather than volume-matched. After concentration analysis of the stock solution, all microbubbles were diluted in PBS to a target concentration of 10^8 bubbles/mL, and final concentration was tested again before data collection. For preclinical acoustic angiography, 10^8 bubbles/mL is a typically employed dose and was therefore chosen as the target concentration for comparison in this work (Lindsey et al. 2017a; Lindsey et al. 2017b; Rao et al. 2016; Shelton et al. 2015).

Ultrasound Parameters and Setup

For this work, a prototype dual-frequency transducer (modified RMV 710, FUJIFILM VisualSonics, Inc., Toronto, ON, Canada) with two confocally-aligned single elements was used (Gessner et al. 2010). At a pulse repetition frequency (PRF) of 20 Hz, a single cycle cosine-windowed sine wave at 4 MHz was transmitted with the low frequency element of this transducer, which has been described in detail previously (Lindsey et al. 2015b). The high frequency element received at 25 MHz, and both elements have a focal depth of 16 mm. This results in transmit and receive beamwidths of approximately 474 μm and 142 μm, respectively. The peak negative pressure of the transmit waveform varied from 400 to 2400 kPa, corresponding to a mechanical index (MI) range of 0.2 to 1.2. This MI range was chosen to cover acoustic pressures that we have explored for superharmonic imaging. Previous studies have demonstrated that acoustic pressures which typically result in microbubble fragmentation result in the greatest superharmonic content, although lower pressures which do not result in immediate bubble fragmentation can also produce weaker superharmonics (Lindsey et al. 2014). A cellulose tube of inner diameter 200 μm was placed at the focal depth of the transducer and aligned perpendicular to the direction of acoustic propagation in a water bath maintained at 37°C (±1°C). The contrast agent of interest was infused through the tube at a rate of 15.9 mm/s using an infusion pump (Pump 11 Elite, Harvard Apparatus, Holliston, MA, USA). With this flow rate, a PRF of 20 Hz, and the beamwidths given above, fresh contrast was insonified with each transmission. Between different trials and contrast agents, the tube was flushed with distilled water until no bubble signal remained.

Data Acquisition and Analysis

To collect raw radiofrequency (RF) data, a custom circuit was built to allow connection of the modified RMV probe to a broadband receive amplifier (Ritec, Inc., Warwick, RI, USA), removing the need for a Vevo770 preclinical ultrasound scanner (FUJIFILM VisualSonics, Inc., Toronto, ON, Canada). Collecting data through a simple receive amplifier was preferable for this work because it allowed greater control over experimental parameters, such as pulse repetition frequency, and removed possible unknown data transformations performed within the scanner. The experimental setup used is depicted in Figure 1. After amplification, the RF data was sampled at 200 MS/s and digitized with a 12-bit digitizer board (CSE1222, DynamicSignals LLC, Lockport, IL, USA) before collection with a custom LabVIEW program (National Instruments Corporation, Austin, TX, USA). For all contrast agents, twelve trials were performed. The twelve trials were split equally among four vials of each contrast agent, with an exception for SIMB1–2, for which only three vials of contrast agent were available. For each trial, a fresh dilution was prepared, the concentration was measured, and 200 lines of RF data were saved for analysis at each pressure. RF data was also saved at each pressure while the tube was infused with water as reference.

To account for the frequency response of the transducer used for data collection, a proxy for the frequency response of the receive element was measured via pulse-echo test on a linear reflector. A steel ball with a diameter of 6.35 mm (44x larger than the beamwidth of the receive element) was placed at the focus of the transducer to be used as a linearly reflecting

target, and a single-cycle 30 MHz pulse was transmitted. The received pulse-echo RF data was sampled, digitized, and recorded as mentioned above. The frequency spectrum was taken as the magnitude of the Fourier transform of the RF data, and the receive frequency response was obtained by taking the square root of the pulse-echo spectrum. The receive bandwidth measured in this way does not provide a full electromechanical and acoustical frequency response, but it is representative of the frequency behavior of the transducer. The measured receive response is depicted in Figure 2.

All analysis was performed in MATLAB (The Mathworks, Inc., Natick, MA, USA). For each line of RF data, the linear frequency spectrum was obtained by taking the magnitude component of the fast Fourier transform of each line. To remove any signal from the tube walls, the average spectrum from water was subtracted from each contrast spectrum. The resulting spectrum was then normalized by the frequency response of the receive element. Superharmonic response was quantified as the area under the curve (AUC) of the normalized, water-subtracted frequency spectrum of the collected data inside the −6 dB bandwidth of the receive element, indicated by the arrow in Figure 2 (8.5 MHz to 35.7 MHz). The AUC metric was calculated by the trapezoidal method and averaged over the 200 lines collected for each agent and pressure. The mean AUC from each trial was then averaged over all trials for the final superharmonic metric, which is presented as mean ± standard error.

Results and Discussion

The mean diameter and concentration of each sample of contrast agent as measured after dilution for concentration-matching are shown in Figure 3. The mean diameter of each contrast agent is shown in Figure 3 (A, C, E, G). Here, the target concentration was 10^8 bubbles/mL. To ensure that each dilution was adequately matched to the target concentration, we characterized the variability of our complete experimental setup. Preliminary data (unpublished) found that a 2.3x increase in concentration led to only a 5% increase in superharmonic AUC, while two independent dilutions of the same concentration produced superharmonic AUCs differing by 7%. This data demonstrates that up to two-fold changes in concentration result in AUC values within the variability of this experimental measurement. The source of this experimental variability may be a combination of variations in the mixing of individual dilutions, small temperature fluctuations in the water bath and surrounding laboratory, variations in concentration measurement on the sizing device used here, among others. As such, the spread of concentrations displayed in Figure 3 (B, D, F, H) was deemed acceptable for this work.

First, the effect of gas core composition on superharmonic energy production by microbubbles was evaluated. The three gases used here (OFP, DFB, and SF_6) are commonly used in the current generation of ultrasound contrast agents, as their high molecular weights improve stability in circulation *in vivo* (de Jong et al. 2009; Kabalnov et al. 1998). Our results, as shown in Figure 4A, indicated greater superharmonic production from either perfluorocarbon-filled agent compared to the SF_6-filled bubbles for MI ≥ 0.6. OFP and DFB bubbles produced superharmonic AUCs of 53.68 ± 4.276 and 46.43 ± 3.805 a.u., respectively, at MI = 1.2, while that produced by SF_6 bubbles was 28.56 ± 1.769 a.u.. SF_6

microbubbles have been shown to exhibit increased resistance to pressure changes, such as those experienced in cardiac flow (Schneider et al. 1995). Due to this increased resistance, a clinically-used SF_6-filled contrast agent has been shown to exhibit longer circulation time compared to Definity and Optison (Hyvelin et al. 2017). The diffusivity and solubility properties of the gas core may have an effect on certain acoustic responses, in addition to microbubble stability; one study reported that bubbles filled with higher diffusion coefficient gases, such as SF_6, exhibited less delayed subharmonic emissions compared to perfluorocarbon-filled bubbles (Kanbar et al. 2017). As such, it is fathomable that other acoustic responses, such as superharmonic production, could also be influenced by properties of the gas core. In addition, the SF_6-filled microbubbles prepared here had a slightly larger mean diameter (1.23 μm) than either OFP-filled (1.00 μm) or DFB-filled (0.92 μm) bubbles, though all three contrast agents were prepared under the same conditions. Due to the inverse relationship between bubble diameter and resonance frequency (de Jong et al. 2009; Kaya et al. 2010), this could have an effect on the resulting acoustic response.

Microbubble contrast agents with different lipid shell compositions were also compared. The results for this group are shown in Figure 4B. Here, we observed greater superharmonic production from the contrast agents with longer acyl chains, C18–2L and C20–2L. At MI = 1.2, C18–2L produced the most superharmonic energy with an AUC of 53.68 ± 4.276 a.u., followed by C20–2L with 46.20 ± 1.565 a.u., C16–3L with 36.04 ± 3.182 a.u., and C16–2L with 25.55 ± 2.524 a.u.. These results agree with those of van Rooij et al. (2015), who reported higher second harmonic responses for bubbles with 18 carbon acyl chains compared to 16 carbon acyl chains. Others have evaluated microbubble stability as a function of acyl chain length and found that as chain length increased from 16 to 22 carbon atoms, stability also increased (Garg et al. 2013). However, the differences in stability observed by Garg et al. (2013) in diluted microbubbles were insignificant at short time scales (i.e. less than 20 minutes in dilution). For the current study, each trial was performed in five minutes or less from time of dilution to completion of data acquisition. As such, any effects of stability should be negligible in the current results.

The clinical and preclinical contrast agents compared in this work were Definity, Optison, and Micromarker (Table I). Definity and Optison are both approved for clinical use in the United States, while Micromarker is solely a preclinical agent. While Definity and Micromarker have phospholipid shells, Optison is protein-shelled (Vevo Micromarker booklet; Optison package insert 2016; Definity package insert 2017). To reach 10^8 bubbles/mL, Definity required a 0.68% dilution from the measured stock concentration of 1.51×10^{10} bubbles/mL, while Optison required a 23.8% dilution from the measured stock concentration of 4.21×10^8 bubbles/mL. These values may be of interest to others who use these commercially available, clinical contrast agents. The results of the comparison of this group are shown in Figure 4C. The superharmonic response of Optison behaved asymptotically above MI = 0.8, while Micromarker and Definity increased relatively linearly throughout the mechanical index range tested. At MI = 1.2, the maximum MI tested, the superharmonic AUC of Optison was 17.79 ± 2.013 arbitrary units (a.u.), nearly three times less than that of Definity (48.67 ± 4.712 a.u.) or Micromarker (52.84 ± 2.285 a.u.). At a more intermediate MI = 0.6, Optison produced an AUC of 7.96 ± 0.661 a.u., only half that of Definity (15.67 ± 1.75 a.u.) or Micromarker (18.42 ± 0.584 a.u.). Similar trends were

observed between Optison and Definity in a comparative study of clinical ultrasound contrast agents (Hyvelin et al. 2017).

The relatively poor performance of Optison compared to these other agents is likely due to two factors: 1) its albumin shell and 2) larger size distribution. Albumin-shelled microbubbles have been found to be more susceptible to static diffusion and less susceptible to shell fragmentation at acoustic pressures below 800 kPa compared to phospholipid-shelled microbubbles (Chomas et al. 2001). This could have negative implications for superharmonic imaging with albumin-shelled bubbles based on previous work demonstrating that superharmonic signals are preferentially generated by microbubbles undergoing substantial oscillations and that these signals are largest when these oscillations lead to fragmentation (Lindsey et al. 2015a). Furthermore, in this work, Optison had a mean diameter of 2.94 μm, compared to 0.96 μm for Definity and 0.99 μm for Micromarker (Figure 3G). The effect of microbubble diameter on superharmonic signal production is discussed in the following paragraphs.

Size-isolated microbubbles (SIMBs, Advanced Microbubbles Laboratories, LLC, Boulder, CO, USA) were used to compare the superharmonic response of microbubbles with the same shell and gas properties but different diameters (Table I). The diameters tested ranged from 1.34 μm to 3.78 μm (Figure 3E). Results are shown in Figure 4D. Superharmonic AUC generally decreased as bubble diameter increased, with the smaller SIMBs performing similarly and producing greater superharmonic signal than the larger SIMBs. For example, at MI = 1.2, AUC values of 33.59 ± 2.881, 29.14 ± 3.331, 17.36 ± 2.455, and 9.40 ± 1.061 a.u. were obtained for SIMB 1–2, 3–4, 4–5, and 5–8, respectively. As MI increases, the difference in superharmonic production between the groups (particularly SIMB 1–2 and 3–4 versus SIMB 4–5 and 5–8) became more exaggerated. As previously discussed, bubble diameter is inversely related to resonance frequency, which likely contributes to the differences in superharmonic AUC observed among these groups. As bubble diameter increased, resonance frequency decreased, moving the insonification frequency further from resonance. Kaya et al. (2010) performed a comprehensive study on the acoustic responses of monodisperse microbubbles with different diameters and demonstrated the importance of coupling excitation frequency to microbubble resonance. These studies demonstrated via simulation and experiment that larger bubbles (6–8 μm diameter) resonate and produce their largest response around 1 MHz, while smaller bubbles (2–4 μm diameter) produce greater responses near resonance between 3–6 MHz (Kaya et al. 2010).

Previous work by our group has elucidated the origins of superharmonic signal production (Lindsey et al. 2015a). The authors determined that the strongest superharmonic signals are produced by oscillations resulting in microbubble shell fragmentation, and that such fragmentation occurs preferentially for smaller bubbles (1 μm) on the initial insonifying pulse, while larger bubbles (4 μm) are prone to shrinking, which persists over several pulses, producing weaker superharmonic signals (Lindsey et al. 2015a). Moreover, for stationary bubbles, 1 μm bubbles initially produced greater superharmonic intensity, which decayed quickly to a lower value than that produced by 4 μm bubbles (Lindsey et al. 2015a). In the current work, all data was acquired while contrast was flowing, so signal decay was not

observed, and smaller bubbles consistently produced greater superharmonic signals than larger bubbles. Our results therefore agree with those of Lindsey and colleagues.

However, other studies have suggested increases in scattered signal when using larger bubbles (Lin et al. 2017; Sirsi et al. 2010; Streeter et al. 2010; Talu et al. 2008), due to the dependence of scattering cross section on microbubble radius (Dayton et al. 1999). For example, Streeter et al. (2010) showed increased molecular targeting signal using 3 μm bubbles over 1 μm bubbles with a 7 MHz harmonic imaging scheme, while Sirsi and colleagues (2010) used 6–8 μm bubbles to enhance fundamental imaging at 40 MHz. It is obvious that there are many interconnected factors influencing the results of these previous works and the current study, including microbubble composition, size, the frequencies at which bubbles are excited, and the bandwidth at which bubble echoes are received. Future work is needed to continue illuminating these relationships, as the current study is limited to the specific 4 MHz excitation case with a receive bandwidth between 8.5–35.7 MHz.

While all contrast agents were tested at a matched concentration in this work, clinical contrast agents are not necessarily used at the same concentration or dose. For example, the stock concentration and the clinically recommended doses for Definity and Optison are different. The recommended doses for one bolus of Definity and Optison are 10 μL/kg (Definity package insert 2017) and 0.5 mL (Optison package insert 2016), respectively. Assuming an average male patient as described by the US Center for Disease Control and Prevention (Fryar et al. 2012) and using Nadler's formula to calculate blood volume (Nadler et al. 1962), we can estimate a typical clinical concentration for these contrast agents. Consider a fictional patient who weighs 88.7 kg and has a blood volume of 5.46 L. Assuming a stock concentration of 1.2×10^{10} bubbles/mL (Definity package insert 2017), the overall concentration of Definity in circulation after one bolus at the recommended dose would be 1.9×10^{6} bubbles/mL. In the same patient, one bolus of Optison at a stock concentration of 8.0×10^{8} bubbles/mL (Optison package insert 2016) would result in an overall concentration of 7.3×10^{4} bubbles/mL – two orders of magnitude lower than that of Definity. If the results observed for these two clinical agents in the present study can be extrapolated to lower concentrations, this difference in dose could be discouraging for clinical superharmonic imaging with Optison. However, concentration is known to play a significant role in microbubble behavior under acoustic stimulation, as discussed in the following section.

Limitations

A main limitation of the present study is the relatively high concentration used during data collection. While this concentration is relevant for preclinical imaging, it is known that higher microbubble concentrations lead to greater bubble-bubble interactions (Yasui et al. 2009). Specifically, high bubble concentrations result in smaller distances between individual microbubbles in a field, which decreases the overall resonance frequency of the bubble population; this has been shown both theoretically (Feuillade 1995; Morioka 1974; Weston 1966) and experimentally (Hsiao et al. 2001; Payne et al. 2007). This implies that the results of the present work may not simply extrapolate to lower concentrations, such as

those used in the clinic, and further investigation may be necessary to continue improvement of clinical superharmonic contrast imaging.

Another important limitation of this work is the method used for concentration matching. The particle sizing device used here to obtain concentration and size measurements is inherently limited to measure particles between 0.5 and 400 μm (Accusizer product note 2014). As such, the concentration of a polydisperse contrast agent with significant portions of its distribution outside this range will be measured inaccurately by this device. It is unlikely that ultrasound contrast agents contain bubbles larger than 400 μm in diameter, but it is feasible that polydisperse agents with a mean diameter around 1 μm, such as Definity, Micromarker, and our in-house formulations, have populations of bubbles below 0.5 μm in size. If so, the concentrations of these agents would be misrepresented to be lower than they truly are, which could explain the differences, or lack thereof, in superharmonic signal generation we have observed in these agents. This methodology also affects the mean diameter of different microbubbles measured in this work. The values reported here may appear lower than those reported in other literature, due to the minimum detection threshold of the Accusizer (0.5 μm), compared to other common methodologies, such as a Coulter Counter or optical microscopy sizing. Furthermore, the values reported here are number-weighted rather than volume-weighted. The methodology used in measuring and reporting microbubble size is a major confounding variable that should always be considered in the interpretation of experimental results where bubble size is reported.

This study focused on the effect of different properties of microbubble contrast agents on superharmonic signal production. Recently, attention has been brought to the importance of properties of the external environment when assessing the acoustic response of microbubbles. Others have reported decreased microbubble oscillation amplitude (Helfield et al. 2016b) and fragmentation (Helfield et al. 2016a) in fluids with viscosities similar to blood. Helfield et al. (2016a) also observed a decrease in broadband superharmonic emissions, in keeping with the observation by Lindsey et al. (2015a) that substantial broadband superharmonic signals originate from microbubble fragmentation. Because the current work used a less viscous fluid during data collection, the superharmonic content recorded is likely much greater than would be seen *in vivo*. While the absolute values of the superharmonic metric used here would decrease, we believe the trends shown would remain valid in a blood-like fluid.

Many studies have examined the behavior of microbubbles in capillary-sized tubes. It has been reported that bubbles in 12–25 μm inner diameter tubes produce smaller oscillation amplitudes (Caskey et al. 2006; Thomas et al. 2013) and exhibit fewer occurrences of microbubble fragmentation (Caskey et al. 2006) than those in 160–200 μm tubes. Furthermore, Sassaroli and Hynynen (2006) have shown that the acoustic pressure threshold to cause fragmentation increases as tube size decreases. In consequence, the results presented in this work are dependent on the tube used for data collection. The *in vitro* results shown here for a 200 μm synthetic vessel may not translate directly *in vivo*, where a distribution of vessel diameters is present.

Finally, we reiterate that data presented herein is specific to superharmonic imaging within the conditions of the custom fabricated dual-frequency transducer used, which has a frequency bandwidth quite different than current clinical transducers. Hence, observations of microbubble performance observed here should not be assumed to exhibit the same trends for pulse inversion, amplitude modulation, subharmonic imaging, or other techniques performed within the bandwidth of commercial clinical transducers and ultrasound systems. Future work will be necessary to evaluate the performance of different contrast agents within clinical imaging parameters. Similarly, additional work will need to be performed to optimize contrast agents for *in vivo* acoustic angiography.

Conclusion

In this work, we have assessed the superharmonic response of several types of contrast agents specific to superharmonic imaging at 4 MHz. We have found that certain microbubbles produce much more superharmonic energy than others when insonified at 4 MHz. In summary, bubbles with perfluorocarbon cores produce more superharmonic content than those with sulfur hexafluoride. Microbubbles with longer acyl chains (18–20 carbons) in the lipid shell create more superharmonic energy than bubbles with shorter chains (16 carbons). Superharmonic production generally decreases with increasing size between 1 and 4 μm, presumably due to decreasing resonance frequency or susceptibility to fragmentation. Finally, Definity and Micromarker may be better suited for clinical and preclinical superharmonic imaging, respectively, than Optison when insonifying at 4 MHz. These results will be used to optimize future acoustic angiography studies and improve contrast-to-tissue ratio and sensitivity. Continuation of this work will include evaluation of these results in animal models *in vivo*.

Acknowledgments

Funding for this work was provided by National Institutes of Health R01 CA189479. I.G.N. was partially funded by National Institutes of Health T32 HL069768. The authors thank Thomas Winter for building the custom circuit and James Tsuruta and Brian Velasco for contrast agent formulation. Competing interest: P.A.D. is an inventor on a patent describing dual-frequency imaging and acoustic angiography and a co-founder of SonoVol, Inc., which has licensed this patent. The authors appreciate the efforts of F. Stuart Foster, Mark Lukacs, Mike Lee, Emmanuel Cherin, and Chris Chaggares for design of these custom dual-frequency RMV probes.

References

Abou-Elkacem L, Bachawal SV, Willmann JK. Ultrasound Molecular Imaging: Moving Towards Clinical Translation. Eur J Radiol 2015 [cited 2018 Sep 6];84:1685–1693. [PubMed: 25851932]

Accusizer: Single particle optical sizing. 2014 Particle Sizing Systems, Santa Barbara, CA, USA.

Booklet I. Vevo MicroMarker ™ Non-Targeted Contrast Agent Kit : Booklet Contents : MicroMarker Kit Contents:1–9.

Bouakaz A, Frigstad S, Ten Cate FJ, Jong NDE. SUPER HARMONIC IMAGING: A NEW IMAGING TECHNIQUE FOR IMPROVED CONTRAST DETECTION. Ultrasound Med Biol 2002;28:59–68. [PubMed: 11879953]

Caskey CF, Kruse DE, Dayton PA, Kitano TK, Ferrara KW. Microbubble oscillation in tubes with diameters of 12, 25, and 195 microns. Appl Phys Lett 2006;88:1–3.

Chomas JE, Dayton P, Alien J, Morgan K, Ferrara KW. Mechanisms of contrast agent destruction. IEEE Trans Ultrason Ferroelectr Freq Control 2001;48:232–248. [PubMed: 11367791]

Dayton PA, Morgan KE, Klibanov a L, Brandenburger GH, Ferrara KW. Optical and acoustical observations of the effects of ultrasound on contrast agents. IEEE Trans Ultrason Ferroelec, Freq Contr 1999;46:220–232.

de Jong N, Emmer M, van Wamel A, Versluis M. Ultrasonic characterization of ultrasound contrast agents. Med Biol Eng Comput 2009;47:861–873. [PubMed: 19468770]

Definity Package Insert. 2017 Lantheus Medical Imaging, Inc., North Billerica, MA, USA.

Eckersley RJ, Chin CT, Burns PN. Optimising phase and amplitude modulation schemes for imaging microbubble contrast agents at low acoustic power. Ultrasound Med Biol 2005;31:213–219. [PubMed: 15708461]

Feingold S, Gessner R, Guracar IM, Dayton PA. Quantitative volumetric perfusion mapping of the microvasculature using contrast ultrasound. Invest Radiol 2010;45.

Feshitan JA, Chen CC, Kwan JJ, Borden MA. Microbubble size isolation by differential centrifugation. J Colloid Interface Sci Elsevier Inc., 2009;329:316–324.

Feuillade C. Scattering from collective modes of air bubbles in water and the physical mechanism of superresonances. J Acoust Soc Am 1995;98:1178–1190.

Frinking PJA, Bouakaz A, Kirkhorn J, Ten Cate FJ, De Jong N. Ultrasound contrast imaging: Current and new potential methods. Ultrasound Med Biol 2000;26:965–975. [PubMed: 10996696]

Fröhlich E, Muller R, Cui X-W, Schreiber-Dietrich D, Dietrich CF. Dynamic Contrast-Enhanced Ultrasound for Quantification of Tissue Perfusion. J Ultrasound Med 2015;34:179–196. [PubMed: 25614391]

Fryar CD, Gu Q, Ogden CL. Anthropometric reference data for children and adults: United States, 2007–2010. Vital Heal Stat 2012;1–40.

Garg S, Thomas AA, Borden MA. The effect of lipid monolayer in-plane rigidity on in vivo microbubble circulation persistence. Biomaterials 2013;34:6862–6870. [PubMed: 23787108]

Gessner R, Lukacs M, Lee M, Cherin E, Foster FS, Dayton PA. High-Resolution, High-Contrast Ultrasound Imaging Using a Prototype Dual-Frequency Transducer : In Vitro and In Vivo Studies. IEEE Trans Ultrason Ferroelectr Freq Control 2010;57:1772–1781. [PubMed: 20679006]

Gessner RC, Aylward SR, Dayton PA. Mapping Microvasculature with Acoustic Angiography Yields Quantifiable Differences between Healthy and Tumor-bearing Tissue Volumes in a Rodent Model. Radiology 2012;264:733–740. [PubMed: 22771882]

Gessner RC, Frederick CB, Foster FS, Dayton PA. Acoustic Angiography: A New Imaging Modality for Assessing Microvasculature Architecture. Int J Biomed Imaging, 2013;936593. [PubMed: 23997762]

Gramiak R, Shah PM. Echocardiography of the aortic root. Invest Radiol 1968;3:356–366. [PubMed: 5688346]

Helfield B, Black JJ, Qin B, Pacella J, Chen X, Villanueva FS. Fluid Viscosity Affects the Fragmentation and Inertial Cavitation Threshold of Lipid-Encapsulated Microbubbles. Ultrasound Med Biol 2016a;42:782–794. [PubMed: 26674676]

Helfield B, Chen X, Qin B, Villanueva FS. Individual lipid encapsulated microbubble radial oscillations: Effects of fluid viscosity. J Acoust Soc Am 2016b;139:204–214. [PubMed: 26827018]

Hsiao PY, Devaud M, Bacri JC. Acoustic coupling between two air bubbles in water. Eur Phys J E 2001;4:5–10.

Hudson JM, Karshafian R, Burns PN. Quantification of Flow Using Ultrasound and Microbubbles: A Disruption Replenishment Model Based on Physical Principles. Ultrasound Med Biol 2009;35:2007–2020. [PubMed: 19822390]

Hyvelin J-M, Gaud E, Costa M, Helbert A, Bussat P, Bettinger T, Frinking P. Characteristics and Echogenicity of Clinical Ultrasound Contrast Agents: An In Vitro and In Vivo Comparison Study. J Ultrasound Med 2017;36:941–953. [PubMed: 28240842]

Kabalnov A, Bradley JA, Flaim S, Klein D, Pelura T, Peters B, Otto S, Reynolds J, Schutt E, Weers J. Dissolution of multicomponent microbubbles in the bloodstream: 2. Experiment. Ultrasound Med Biol 1998;24:751–760. [PubMed: 9695278]

Kanbar E, Fouan D, Sennoga CA, Doinikov AA, Bouakaz A. Impact of Filling Gas on Subharmonic Emissions of Phospholipid Ultrasound Contrast Agents. Ultrasound Med Biol 2017;43:1004–1015. [PubMed: 28214036]

Kaufmann BA, Lewis C, Xie A, Mirza-Mohd A, Lindner JR. Detection of recent myocardial ischaemia by molecular imaging of P-selectin with targeted contrast echocardiography. Eur Heart J 2007;28:2011–2017. [PubMed: 17526905]

Kaya M, Feingold S, Hettiarachchi K, Lee AP, Dayton PA. Acoustic responses of monodisperse lipid-encapsulated microbubble contrast agents produced by flow focusing. Bubble Sci Eng Technol 2010;2:33–40. [PubMed: 21475641]

Kruse DE, Ferrara KW. A new imaging strategy using wideband transient response of ultrasound contrast agents. IEEE Trans Ultrason Ferroelectr Freq Control 2005;52:1320–1329. [PubMed: 16245601]

Lee HJ, Yoon T-J, Yoon Y Il. Synthesis of ultrasound contrast agents: characteristics and size distribution analysis (secondary publication). Ultrasonography 2017;36:378–384. [PubMed: 28290183]

Lin F, Tsuruta JK, Rojas JD, Dayton PA. Optimizing Sensitivity of Ultrasound Contrast-Enhanced Super-Resolution Imaging by Tailoring Size Distribution of Microbubble Contrast Agent. Ultrasound Med Biol 2017;43:2488–2493. [PubMed: 28668636]

Lindsey BD, Rojas JD, Dayton PA. On the Relationship Between Microbubble Fragmentation, Deflation and Broadband Superharmonic Signal Production. Ultrasound Med Biol 2015a;41:1711–1725. [PubMed: 25766572]

Lindsey BD, Rojas JD, Martin KH, Shelton SE, Dayton PA. Acoustic characterization of contrast-to-tissue ratio and axial resolution dual-frequency contrast-specific “acoustic angiography” imaging. IEEE Trans Ultrason Ferroelec, Freq Contr 2014;61:1668–1687.

Lindsey BD, Shelton SE, Dayton PA. OPTIMIZATION OF CONTRAST-TO-TISSUE RATIO THROUGH PULSE WINDOWING IN DUAL-FREQUENCY “ACOUSTIC ANGIOGRAPHY” IMAGING. Ultrasound Med Biol 2015b;41:1884–1895. [PubMed: 25819467]

Lindsey BD, Shelton SE, Foster FS, Dayton PA. Assessment of Molecular Acoustic Angiography for Combined Microvascular and Molecular Imaging in Preclinical Tumor Models. Mol Imaging Biol Molecular Imaging and Biology, 2017a;19:194–202. [PubMed: 27519522]

Lindsey BD, Shelton SE, Martin KH, Ozgun KA, Rojas JD, Foster FS, Dayton PA. High Resolution Ultrasound Superharmonic Perfusion Imaging: In Vivo Feasibility and Quantification of Dynamic Contrast-Enhanced Acoustic Angiography. Ann Biomed Eng 2017b;45:939–948. [PubMed: 27832421]

Morioka M. Theory of natural frequencies of two pulsating bubbles in infinite liquid. J Nucl Sci Technol 1974;11:554–560.

Optison Package Insert. 2016 GE Healthcare, Inc., Marlborough, MA, USA.

Nadler S, Hidalgo J, Bloch T. Prediction of blood volume in normal human adults. Surgery 1962;51:224–232. [PubMed: 21936146]

Payne EMB, Ooi A, Manasseh R. Symmetric mode resonance of bubbles near a rigid boundary - The nonlinear case with time delay effects. Proc 16th Australas Fluid Mech Conf 16AFMC 2007;1336–1339.

Rao SR, Shelton SE, Dayton PA. The “Fingerprint” of Cancer Extends Beyond Solid Tumor Boundaries: Assessment With a Novel Ultrasound Imaging Approach. IEEE Trans Biomed Eng 2016;63:1082–1086. [PubMed: 26394410]

Sassaroli E, Hynynen K. On the impact of vessel size on the threshold of bubble collapse. Appl Phys Lett 2006;89:1–3.

Schneider M, Arditi M, Barrau MB, Brochot J, Broillet A, Ventrone R, Yan F. BR1: a new ultrasonographic contrast agent based on sulfur hexafluoride-filled micrububbles. Invest Radiol 1995;30:451–457. [PubMed: 8557510]

Segers T, Kruizinga P, Kok MP, Lajoinie G, de Jong N, Versluis M. Monodisperse Versus Polydisperse Ultrasound Contrast Agents: Non-Linear Response, Sensitivity, and Deep Tissue Imaging Potential. Ultrasound Med Biol 2018;44:1482–1492. [PubMed: 29705522]

Shelton SE, Lee YZ, Lee M, Cherin E, Foster FS, Aylward SR, Dayton PA, Dayton P. Quantification of microvascular tortuosity during tumor evolution utilizing acoustic angiography. Ultrasound Med Biol 2015;41:1896–1904. [PubMed: 25858001]

Shelton SE, Lindsey BD, Dayton PA, Lee YZ. First-in-Human Study of Acoustic Angiography in the Breast and Peripheral Vasculature. Ultrasound Med Biol 2017;43:2939–2946. [PubMed: 28982628]

Shen C-C, Chou Y-H, Li P-C. Pulse Inversion Techniques in Ultrasonic Nonlinear Imaging. J Med Ultrasound 2005;13:3–17.

Shi WT, Forsberg F, Hall AL, Chiao RY, Liu J-B, Goldberg ' BB, Miller S, Thomenius KE, Wheatley4 MA. Subharmonic Imaging with Microbubble Contrast Agents: Initial Results. Ultrason Imaging 1999;21:79–94. [PubMed: 10485563]

Sirsi S, Feshitan J, Kwan J, Homma S, Borden M. Effect of Microbubble size on Fundamental Mode High Frequency Ultrasound Imaging in Mice. Ultrasound Med Biol 2010;36:935–948. [PubMed: 20447755]

Sridharan A, Eisenbrey JR, Liu J Bin, Machado P, Halldorsdottir VG, Dave JK, Zhao H, He Y, Park S, Dianis S, Wallace K, Thomenius KE, Forsberg F. Perfusion estimation using contrast enhanced three-dimensional subharmonic ultrasound imaging: an in vivo study. Invest Radiol 2013;48:654–660. [PubMed: 23695085]

Streeter J, Gessner R, Miles I, Dayton PA. Improving Sensitivity in Ultrasound Molecular Imaging by Tailoring Contrast Agent Size Distribution: In Vivo Studies. Mol Imaging 2010;9:87–95. [PubMed: 20236606]

Talu E, Hettiarachchi K, Zhao S, Powell RL, Lee AP, Longo L, Dayton PA. Tailoring the Size Distribution of Ultrasound Contrast Agents: Possible Method for Improving Sensitivity in Molecular Imaging. 2008;6:384–392.

Thomas DH, Sboros V, Emmer M, Vos H, Jong N. Microbubble oscillations in capillary tubes. IEEE Trans Ultrason Ferroelectr Freq Control 2013;60:105–114. [PubMed: 23287917]

Tsuruta JK, Schaub NP, Rojas JD, Streeter J, Klauber-DeMore N, Dayton P. Optimizing ultrasound molecular imaging of secreted frizzled related protein 2 expression in angiosarcoma. PLoS One 2017;12:e0174281. [PubMed: 28333964]

Van Rooij T, Luan Y, Renaud G, Van Der Steen AFW, Versluis M, De Jong N, Kooiman K. NON-LINEAR RESPONSE AND VISCOELASTIC PROPERTIES OF LIPID-COATED MICROBUBBLES: DSPC VERSUS DPPC. Ultrasound Med Biol 2015;41:1432–1445. [PubMed: 25724308]

Weston DE. Acoustic Interaction Effects in Arrays of Small Spheres. J Acoust Soc Am 1966;39:316–322.

Yasui K, Lee J, Tuziuti T, Towata A, Kozuka T, Iida Y. Influence of the bubble-bubble interaction on destruction of encapsulated microbubbles under ultrasound. J Acoust Soc Am 2009;126:973–982. [PubMed: 19739710]

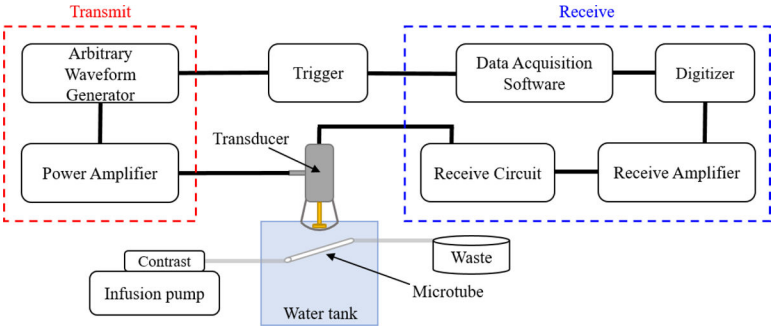

Figure 1: Experimental setup.

Schematic diagram illustrating the experimental setup used in this work.

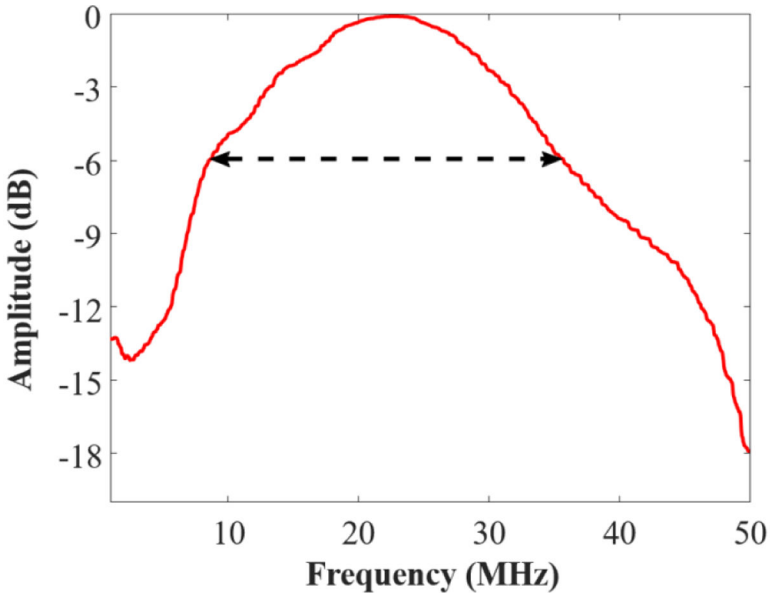

Figure 2: Frequency response of the receive element.

Frequency response of the receive element from 0 to 50 MHz (red) and its – 6 dB bandwidth with cutoff at 8.5 and 35.7 MHz (black dashed arrow).

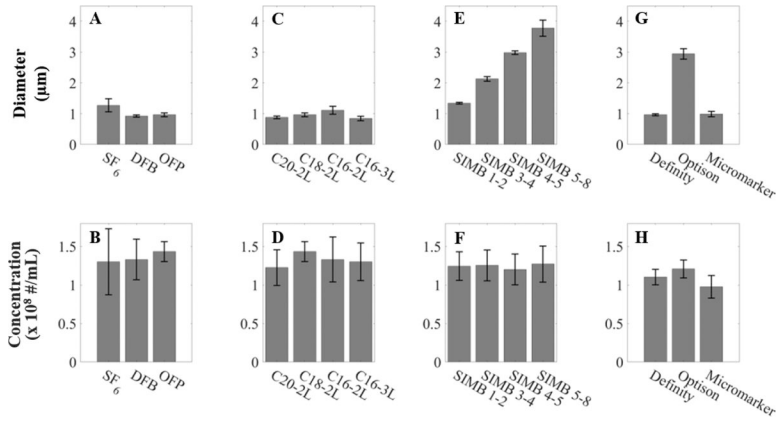

Figure 3: Size and concentration of the contrast agents used in this work.

Size (A, C, E, G) and concentration (B, D, F, H) measurements for the contrast agents used in each group: gas core (A-B), lipid shell (C-D), bubble diameter (E-F), and clinical and preclinical (G-H). Data are presented as mean ± standard deviation for n = 12 trials per contrast agent.

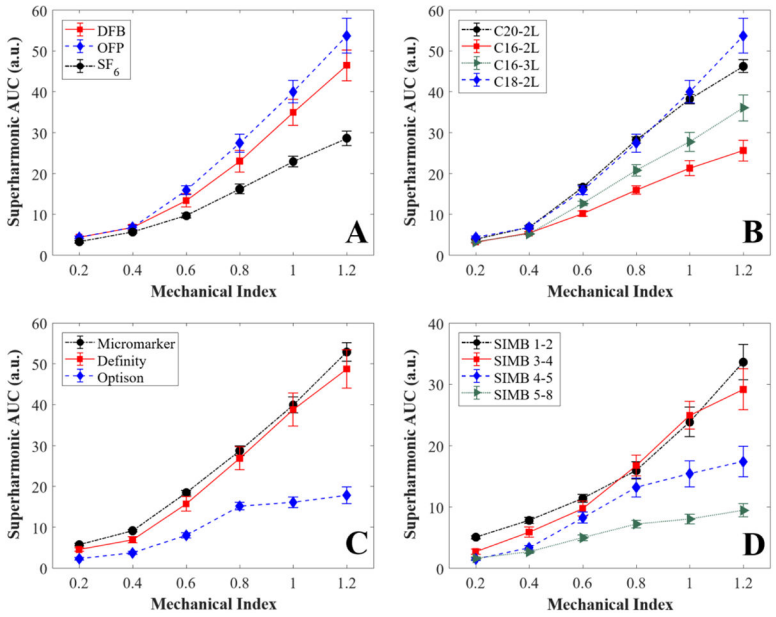

Figure 4: Summary of results.

Comparison of: A) clinical and preclinical contrast agents, B) contrast agents with different gas cores, C) contrast agents with different lipid shell compositions, and D) contrast agents with different bubble diameters. Data are presented as mean ± standard error for n = 12 trials per contrast agent. AUC = area under the curve, OFP = octafluoropropane, DFB = decafluorobutane, SF_6 = sulfur hexafluoride.

Table 1.

Summary of contrast agents.

Group	Name	Shell	Core	Size Distribution	Manufacturer
Clinical and Preclinical	Definity	lipid	octafluoropropane	polydisperse	Lantheus Medical Imaging
	Optison	protein	octafluoropropane	polydisperse	GE Healthcare
	Micromarker	lipid	nitrogen and decafluorobutane	polydisperse	FUJIFILM VisualSonics, Inc.
Gas Core	DFB	lipid	decafluorobutane	polydisperse	Dayton Lab
	OFP	lipid	octafluoropropane	polydisperse	Dayton Lab
	SF_6	lipid	sulfur hexafluoride	polydisperse	Dayton Lab
Lipid Shell	C16-2L	lipid	octafluoropropane	polydisperse	Dayton Lab
	C20-2L	lipid	octafluoropropane	polydisperse	Dayton Lab
	C16-3L	lipid	octafluoropropane	polydisperse	Dayton Lab
	C18-2L	lipid	octafluoropropane	polydisperse	Dayton Lab
Bubble Diameter	SIMB1-2	lipid	decafluorobutane	size-sorted	Advanced Microbubbles Laboratories
	SIMB3-4	lipid	decafluorobutane	size-sorted	Advanced Microbubbles Laboratories
	SIMB4-5	lipid	decafluorobutane	size-sorted	Advanced Microbubbles Laboratories
	SIMB5-8	lipid	decafluorobutane	size-sorted	Advanced Microbubbles Laboratories

Table 2.

In-house lipid formulations.

Name	Acyl Chain Length	Number of Lipids	Lipid Composition	Molar Ratio	Propylene Glycol (vol%)	Glycerol (vol%)
C16-2L	16	2	DPPC:DPPE-PEG2000	9:1	15	5
C20-2L	20	2	DAPC:DSPE-PEG2000	9:1	15	5
C16-3L	16	3	DPPC:DPPA:DPPE-PEG5000	8.2:1:0.5	10	10
C18-2L	18	2	DSPC:DSPE-PEG2000	9:1	15	5

Abbreviations:
DPPC = dipalmitoylphosphatidyl-choline
DPPE = dipalmitoylphosphatidyl-ethanolamine
DPPA = dipalmitoyl-phosphate
DSPC = distearoylphosphatidyl-choline
DSPE = distearoylphosphatidyl-ethanolamine
DAPC = diarachidonoylphosphatidyl-choline
PEG = polyethylene glycol